New Robust Bleomycin Analogues: Synthesis, Spectroscopy, and Crystal Structures of the Copper(II) Complexes

Hiromasa Kurosaki,[†] Kentarou Hayashi,[†] Yoshinobu Ishikawa,[†] Masafumi Goto,*[,†] Kazufumi Inada,[‡] Isao Taniguchi,[‡] Mitsuhiko Shionoya,[§] and Eiichi Kimura*[,||]

Faculty of Pharmaceutical Sciences, Kumamoto University, Oe-honmachi 5-1, Kumamoto 862, Japan, Department of Applied Chemistry and Biochemistry, Kumamoto University, Kurokami 2-39-1, Kumamoto 860, Japan, Institute for Molecular Science, Myodaiji, Okazaki 444, Japan, and Department of Medicinal Chemistry, School of Medicine, Hiroshima University, Kasumi 1-2-3, Minami-ku, Hiroshima 734, Japan

Received May 5, 1998

Two new bleomycin analogues, 2-[((2-(4-imidazolyl)ethyl)amino)carbonyl]-6-[((2-amino-2-methylpropyl)amino)-methyl]pyridine = **L_3** and 2-[((2-(4-imidazolyl)ethyl)amino)carbonyl]-6-[((2-amino-1,1,2-trimethylpropyl)amino)-methyl]pyridine = **L_4**, were synthesized in order to create air-stable ligands of their Cu^I (and Fe^{II}) complexes. The protonation constants (log K_n) of the ligands at 25 °C and $I = 0.1$ M $NaNO_3$ were 9.9, 6.9, and 5.2 for **L_3** and 10.0, 6.7, and 3.9 for **L_4**. The complexation of the triprotonated **L_3** and **L_4** with Cu^{II} started at pH < 5 to yield 4-coordinate $[Cu^{II}(H_{-1}L)\cdot H^+]^{2+}$ complexes, **4** and **6**, respectively, followed by formation of square-pyramidal $[Cu^{II}(H_{-1}L)]^+$ complexes, **5** and **7**, with pK_a values of 5.6 for **5** and 5.9 for **7**. The complexation constants, log $K_{Cu^{II}H_{-1}L}$, were 8.9 for $[Cu^{II}(H_{-1}L_3)]^+$, **5**, and 8.6 for $[Cu^{II}(H_{-1}L_4)]^+$, **7**, respectively. The structures of $[Cu^{II}(H_{-1}L_3)]ClO_4$ (**5**·ClO_4) and $[Cu^{II}(H_{-1}L_4)]BF_4$ (**7**·BF_4) were determined by X-ray crystallography. Crystal data for **5**·ClO_4: monoclinic, space group $P2_1/n$ (No. 14), $a = 13.978(6)$ Å, $b = 8.103(3)$ Å, $c = 18.037(5)$ Å, $\beta = 98.61(3)°$, $V = 2019(1)$ Å^3, $Z = 4$, $R = 0.053$, and $R_w = 0.044$ for 2996 [$I > 3\sigma(I)$] reflections. Crystal data for **7**·BF_4: monoclinic, space group $P2_1/n$ (No. 14), $a = 16.092$ (4) Å, $b = 7.974(4)$ Å, $c = 16.819(2)$ Å, $\beta = 99.64(1)°$, $V = 2127(1)$ Å^3, $Z = 4$, $R = 0.040$, and $R_w = 0.025$ for 1633 [$I > 4\sigma(I)$] reflections. The coordination geometry around the copper was a distorted square-pyramid in **5**, while that of **7** was the intermediate between a trigonal-bipyramid and a square-pyramid. The distortion is influenced strongly by the number of the methyl group. The EPR spectral data for both copper(II) complexes were consistent with the retention of the solid-state structure in frozen DMF/MeOH (1:1) solution at 77 K. The visible absorption spectra of 10% DMF/aqueous solutions (pH 9.5) of **5** and **7** at $I = 0.1$ M $NaNO_3$ showed absorption maxima at 646 nm with a shoulder at ca. 900 nm for **5** and at 658 and 888 nm for **7**. The red-shift of **7** by ca. 12 nm relative to **5** reflects the distortion toward the trigonal-bipyramidal geometry of **7** in solution. Both complexes displayed irreversible redox behavior in DMF at $I = 0.1$ M tetra(*n*-butyl)ammonium tetrafluoroborate. The anodic and cathodic peak potentials obtained by cyclic voltammetry for **5** and **7** were −0.14 and −0.76 V for **5** and −0.17 and −0.80 for **7** vs Ag/AgCl. The cathodic potentials of copper(II) complexes were shifted toward the anodic direction by ca. 20−60 mV compared to the nonsubstituted 5-coordinate, $[Cu^{II}(H_{-1}L_1)]^+$ complex, **16** (−0.82 V vs Ag/AgCl). The Cu^I complexes (**9** and **10**) are air-oxidized to the corresponding Cu^{II} complexes, **5** and **7**, respectively.

Introduction

Since bleomycin (BLM), an antibiotic glycopeptide, has been discovered and isolated as a copper(II) complex from *Streptomyces verticillus* in 1966, BLM has been used clinically for squamous cell carcinoma, malignant lymphoma, and testistumor.[1] BLM chelates Fe^{II} ion and the resulting Fe^{II}−BLM reacts with molecular O_2 to generate an activated oxygen species, which mediates oxidative cleavage of DNA.[2] The DNA degradation by the activated oxygen species has been proposed to commence with abstraction of the C-4′ hydrogen of the deoxyribose moiety of pyrimidine nucleotides adjacent to guanosines.[3]

More recently, the structures of the metal-chelating domain of metallo−BLMs, such as Zn^{II},[4] Cd^{II},[5] Fe^{II},[6] Fe^{II}−CO,[7] and

[†] Faculty of Pharmaceutical Sciences, Kumamoto University.
[‡] Department of Applied Chemistry and Biochemistry, Kumamoto University.
[§] Institute for Molecular Science.
[||] Hiroshima University.

(1) (a) Umezawa, H. In *Bleomycin*: *Current Status and New Developments*; Carter, S. K., Crooke, S. T., Umezawa, H., Eds.; Academic Press: New York, 1978. (b) Hecht, S. M. In *Bleomycin*: *Chemical, Biochemical and Biological Aspects*; Hecht, S. M., Ed.; Springer-Verlag: New York, 1979. (c) Sugiura Y.; Takita, T.; Umezawa, H. *Met. Ions Biol. Syst.* **1985**, *19*, 383.
(2) (a) Sugiura, Y. *J. Am. Chem. Soc.* **1980**, *102*, 5208. (b) Burger, R. M.; Peisach, J.; Horwitz, S. B. *J. Biol. Chem.* **1981**, *256*, 11636. (c) Stubbe, J.; Kozarich, J. W. *Chem. Rev.* **1987**, *87*, 1107. (d) Stubbe, J.; Kozarich, J. W.; Wu., W.; Vanderwall, D. E. *Acc. Chem. Res.* **1996**, *29*, 322. (e) Burger, R. M. *Chem. Rev.* **1998**, *98*, 1153.
(3) (a) Wu, J. C.; Kozarich J. W.; Stubbe, J. *J. Biol. Chem.* **1983**, *258*, 4694. (b) Giloni, L.; Takeshita, M.; Jonson, F.; Iden C.; Grollman, A. P. *J. Biol. Chem.* **1981**, *256*, 8608.
(4) Calafat, A. M.; Won, H.; Marzilli, L. G. *J. Am. Chem. Soc.* **1997**, *119*, 3656.
(5) Otvos, J. D.; Antholine, W. E.; Wehrli, S.; Petering, D. H. *Biochemistry* **1996**, *35*, 1458.
(6) Lehmann, T. E.; Ming, L.-J.; Rosen, M. E.; Que, L. Jr. *Biochemistry* **1997**, *36*, 2807.

10.1021/ic980510i CCC: $18.00
Published on Web 05/21/1999

Co^{III},[8] and the interaction with oligonucleotide DNA,[9] including binding, recognition, and regiochemistry have been determined in detail, using NMR spectroscopic methods in conjunction with molecular dynamics calculations. Morever, attempts to elucidate the fundamental role of the individual building block of the BLM molecule have also been made by semisynthetic analogues[10] and simplified synthetic analogues.[11]

Although recent electrospray mass spectrometry (EMS)[12] and X-ray absorption spectroscopy (XAS)[13] studies suggested the activated BLM is a ferric hydroperoxide complex, the question of whether a high-valent iron complex, such as a ferryl (Fe^{IV}═O) or a perferryl (Fe^{V}═O), exists in the oxidative pathway or not remains to be answered conclusively.

Previously, we have synthesized BLM model ligands, $\mathbf{L_1}$ and $\mathbf{L_2}$ (see Chart 1), on the basis of the X-ray crystal structure of the Cu^{II} complex of BLM P3A, a biosynthetic precursor of BLM,[14] and determined their pH−complexation behaviors with Cu^{II} and Fe^{II} in aqueous solution.[15] Comparison between $\mathbf{L_1}$ and $\mathbf{L_2}$ revealed the essential role of the carbamoyl group in the $\mathbf{L_2}$ molecule. In the case of $\mathbf{L_1}$, for example, precipitation of iron oxide was observed above pH 7 upon complexation with Fe^{II}. On the other hand, $\mathbf{L_2}$ formed a 1:1 Fe^{II}−L_2 complex at physiological pH.

Chart 1

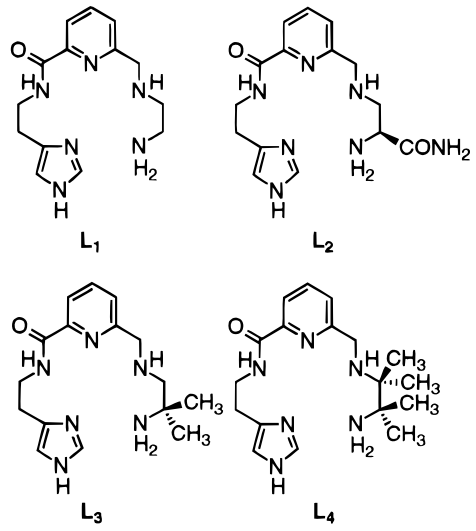

We have also reported the preparation of $Na_2[Fe(CN)_4(1,2\text{-diamine})]$ using 1,2-diamines, such as ethanediamine, *N*-methylethanediamine, and *N*,*N*′-dimethylethanediamine and the dehydrogenation of $Na_2[Fe(CN)_4(1,2\text{-diamine})]$ to yield $Na_2[Fe(CN)_4(1,2\text{-diimine})]$ with oxidizing agents, such as hydrogen peroxide under basic conditions.[16] Supression of the dehydrogenation of ligands is recognized as an important factor in forming high-valent iron complexes.[17] Such ligands will facilitate isolation of a reactive Fe^{II} complex and detection of short-lived high-valent iron complexes formed as intermediates in the oxidative pathway of BLM. To develop the ligands that resist oxidation, we prepared synthetic model ligands, $\mathbf{L_3}$ and $\mathbf{L_4}$, where C−*H*s of the ethanediamine part of $\mathbf{L_1}$ were replaced with C−*CH*$_3$. We have recently reported that the structure of the Zn^{II}−$\mathbf{L_3}$ complex is a 5-coordinate trigonal-bipyramid by X-ray crystallography.[18]

Herein, we report the synthesis and characterization of two new bleomycin model ligands, $\mathbf{L_3}$ and $\mathbf{L_4}$, their complexation properties with Cu^{II}, crystal structures, electronic spectroscopies, and redox properties of their copper(II) complexes, **5** and **7**.

Experimental Section

Materials and General Procedure. The UV−visible absorption measurement was performed on a Shimadzu UV-2200 spectrophotometer, using 1-cm quartz cells. The ^{1}H NMR spectra (270 MHz) were recorded on a JEOL EX-270 spectrometer. Chemical shifts are reported using ppm vs internal standard, tetramethylsilane (TMS) in $CDCl_3$. IR spectra (KBr pellets) were obtained on a JEOL GIR-6500 spectrophotometer. EPR spectra of the frozen DMF/MeOH (1:1 v/v) solutions at

(7) (a) Akkerman, M. A. J.; Haasnoot, C. A. G.; Hiblers, C. W. *Eur. J. Biochem.* **1988**, *173*, 211. (b) Akkerman, M. A. J.; Neijman, E. W. J. F.; Wijmenga, S. S.; Hilbers, C. W. Bermel, W. *J. Am. Chem. Soc.* **1990**, *112*, 7462.

(8) (a) Xu, R. X.; Nettesheim, D.; Otvos, J. D.; Petering, D. H. *Biochemistry* **1994**, *33*, 907. (b) Caceres-Cortes, J.; Sugiyama, H.; Ikudome, K.; Saito, I.; Wang, A. H.-J. *Eur. J. Biochem.* **1997**, *244*, 818.

(9) (a) Wu, W.; Vanderwall, D. E.; Stubbe, J.; Kozarich, J. W.; Turner, C. J. *J. Am. Chem. Soc.* **1994**, *116*, 10843. (b) Manderville, R. A.; Ellena, J. F.; Hecht, S. M. *J. Am. Chem. Soc.* **1994**, *116*, 10851. (c) Manderville, R. A.; Ellena, J. F.; Hecht, S. M. *J. Am. Chem. Soc.* **1995**, *117*, 7981. (d) Wu, W.; Vanderwall, D. E.; Lui, S. M., Tang, X.-J.; Turner, C. J.; Kozarich, J. W.; Stubbe, J. *J. Am. Chem. Soc.* **1996**, *118*, 1268. (e) Wu, W.; Vanderwall, D. E.; Turner, C. J.; Kozarich, J. W.; Stubbe, J. *J. Am. Chem. Soc.* **1996**, *118*, 1281. (f) Lui, S. M.; Vanderwall, D. E.; Wu, W.; Tang, X.-J.; Turner, C. J.; Kozarich, J. W.; Stubbe, J. *J. Am. Chem. Soc.* **1997**, *119*, 9603. (g) Wu, W.; Vanderwall, D. E.; Teramoto, S.; Lui, S. M.; Hoehn, S. T.; Tang, X.-J.; Turner, C. T.; Boger, D. L.; Kozarich, J. W.; Stubbe, J. *J. Am. Chem. Soc.* **1998**, *120*, 2239. (h) Sucheck, S. J.; Ellena, J. F.; Hecht, S. M. *J. Am. Chem. Soc.* **1998**, *120*, 7450.

(10) (a) Oppenheimer, N. J.; Chang, C.; Chang, L.-H.; Ehrenfeld, G.; Rodrigues, L. O.; Hecht, S. M. *J. Biol. Chem.* **1982**, *257*, 1606. (b) Sugiura, Y.; Suzuki, T.; Otsuka, M.; Kobayashi, S.; Ohno, M.; Takita, T.; Umezawa, H. *J. Biol. Chem.* **1983**, *258*, 1328. (c) Sugiyama, H.; Ehrenfeld, G. M.; Shipley, J. B.; Kiluskie, R. E.; Chang, L.-H.; Hecht, S. M. *J. Nat. Prod.* **1985**, *48*, 869. (d) Morii, T.; Saito, I.; Matsuura, T.; Kuwahara, J.; Sugiura, Y. *J. Am. Chem. Soc.* **1987**, *109*, 938. (e) Boger, D. L.; Teramoto, S.; Zhou, J. *J. Am. Chem. Soc.* **1995**, *117*, 7344. (f) Boger, D. L.; Ramsey, T. M.; Cai, H.; Hoehn, S.; Kozarich, J. W.; Stubbe, J. *J. Am. Chem. Soc.* **1998**, *120*, 53. (g) Boger, D. L.; Ramsey, T. M.; Cai, H.; Hoehn, S. T.; Stubbe, J. *J. Am. Chem. Soc.* **1998**, *120*, 9139

(11) (a) Otsuka, M.; Kittaka, A.; Ohno, M.; Suzuki, T.; Kuwahara, J.; Sugiura, Y.; Umezawa, H. *Tetrahedron Lett.* **1986**, *27*, 3639. (b) Otsuka, M.; Masuda, T.; Haupt, A.; Ohno, M.; Shiraki, T.; Sugiura, Y.; Maeda, K. *J. Am. Chem. Soc.* **1990**, *112*, 838. (c) Tan, J. D.; Hudson, S. E.; Brown, S. J.; Olmstead, M. M.; Mascharak, P. K. *J. Am. Chem. Soc.* **1992**, *114*, 3841. (d) Hamamichi, N.; Natrajan, A.; Hecht, S. M. *J. Am. Chem. Soc.* **1992**, *114*, 6278. (e) Kane, S. A.; Natrajan, A.; Hecht, S. M. *J. Biol. Chem.* **1994**, *269*, 10899. (f) Guajardo, R. J.; Hudson, S. E.; Brown, S. J.; Mascharak, P. K. *J. Am. Chem. Soc.* **1993**, *115*, 7971. (g) Quada, J. C.; Levy, M. J.; Hecht, S. M. *J. Am. Chem. Soc.* **1993**, *115*, 12171. (h) Guajardo, R. J.; Tan, J. D.; Mascharak, P. K. *Inorg. Chem.* **1994**, *33*, 2838. (i) Guajardo, R. J.; Chavez, F.; Farinas, E. T.; Mascharak, P. K. *J. Am. Chem. Soc.* **1995**, *117*, 3883. (j) Loeb, K. E.; Zaleski, J. M.; Westre, T. E.; Guajardo, R. J.; Mascharak, P. K.; Hedman, B.; Hodgson, K. O.; Solomon, E. I. *J. Am. Chem. Soc.* **1995**, *117*, 4545. (k) Farinas, E. T.; Tan, J. D.; Mascharak, P. K. *Inorg. Chem.* **1996**, *35*, 2637.

(12) Sam, J. W.; Tang, X.-J.; Peisach, J. *J. Am. Chem. Soc.* **1994**, *116*, 5250.

(13) Westre, T. E.; Loeb, K. E.; Zaleski, J. M.; Hedman, B.; Hodgson, K. O.; Solomon, E. I. *J. Am. Chem. Soc.* **1995**, *117*, 1309.

(14) Iitaka, Y.; Nakamura, H.; Nakatani, T.; Muraoka, Y.; Fujii, A.; Takita, T.; Umezawa, H. *J. Antibiot.* **1978**, *31*, 1070.

(15) (a) Kurosaki, H.; Anan H.; Kimura, E. *Nippon Kagaku Kaishi* **1988**, 691. (b) Kimura, E.; Kurosaki, H.; Kurogi, Y.; Shionoya, M.; Shiro, M. *Inorg. Chem.* **1992**, *31*, 4314.

(16) (a) Goedken, V. L. *J. Chem. Soc., Chem. Commun.* **1972**, 207. (b) Goto, M.; Takeshita, N.; Kanda, N.; Sakai, T.; Goedken, V. L. *Inorg. Chem.* **1985**, *24*, 582. (c) Goto, M.; Takeshita, M.; Sakai, T. *Bull. Chem. Soc.* **1983**, 2051. (d) Ferreira, A. M. C.; Toma, H. E. *J. Chem. Soc., Dalton Trans.* **1983**, 2051. (e) Kuroda, Y.; Tanaka, N.; Goto, M.; Sakai, T. *Inorg. Chem.* **1989,** *28*, 2163.

(17) Collins, T. J.; Fox, B. G.; Hu, Z. G.; Kostka, K. L.; Münck, E.; Rickard, C. E. F.; Wright, L. J. *J. Am. Chem. Soc.* **1992**, *114*, 8724.

(18) Kurosaki, H.; Hayashi, K.; Ishikawa, Y.; Goto, M. *Chem. Lett.* **1995**, 691.

77 K were recorded on a JEOL TE-200 spectrometer, using Mn^{II}-doped MgO powder as a reference ($g_3 = 2.034$ and $g_4 = 1.981$). $Cu(ClO_4)_2 \cdot 6H_2O$ was obtained from Katayama Kagaku and 2-methylpropane-1,2-diamine and tetra(*n*-butyl)ammonium tetrafluoroborate ($TBABF_4$) were obtained from Tokyo Kasei. 2-[((2-(4-(*N*-Triphenylmethylimidazolyl))-ethyl)amino)carbonyl]-6-chloromethylpyridine, **1**,[15] and 2,3-dimethylbutane-2,3-diamine[19] were prepared according to the published methods. Thin-layer chromatography (TLC) and column chromatography were carried out on a Merck Art. 5567 TLC plate (silica gel 60 F_{254}) and Wakogel C-300 (silica gel), respectively. Anion-exchange column chromatography was carried out on Amberlite IRA-400.

Ligand Syntheses. 2-[((2-(4-(*N*-Triphenylmethyl)imidazolyl)-ethyl)amino)carbonyl]-6-[((2-amino-2-methylpropyl)amino)methyl]-pyridine (2). A solution of **1** (6.04 g, 12.30 mmol) and 2-methylpropane-1,2-diamine (10.25 g, 116.28 mmol) in 100 mL of THF was heated at reflux for 4 days and concentrated in vacuo. The remaining residue was purified by chromatography on silica gel (eluent, 10:2:0.2 → 10:1:0.1 $CHCl_3/CH_3OH$/28% aqueous NH_3) to obtain **2** (2.44 g, 37% based on **1**) as a colorless powder. ^1H NMR ($CDCl_3$): δ 1.08 (s, 6H), 1.69 (br, 3H), 2.44 (s, 2H), 2.87 (t, $J = 6.8$ Hz, 2H), 3.75 (q, $J = 6.3$ Hz, 2H), 3.93 (s, 2H), 6.63 (s, 1H), 7.10−7.30 (m, 15H), 7.39 (s, 1H), 7.45 (d, $J = 7.6$ Hz, 1H), 7.78 (dd, $J = 7.6$ Hz, 1H), 8.04 (d, $J = 7.6$ Hz, 1H), 8.69 (br, 1H).

2-[((2-(4-Imidazolyl)ethyl)amino)carbonyl]-6-[((2-amino-2-methylpropyl)amino)methyl]pyridine (L_3). To a solution of **2** (2.44 g, 4.37 mmol) in 100 mL of CH_3OH was added 1 mL of concentrated HCl dropwise. The solution was heated at reflux for 3 h and concentrated in vacuo. The residue was dissolved in 0.5 M HCl (3 mL) and washed with CH_2Cl_2 (50 mL). The aqueous layer was evaporated to dryness. The residue was neutralized by Amberlite IRA-400 resin, and the eluate was concentrated to yield $\mathbf{L_3}$ as a brown solid (1.11 g, 82%). ^1H NMR ($CDCl_3$): δ 1.13 (s, 6H), 2.47 (s, 2H), 2.88 (br, 3H), 2.94 (t, $J = 6.3$ Hz, 2H), 3.74 (t, $J = 6.3$ Hz, 2H), 3.94 (s, 2H), 6.85 (s,1H), 7.39 (d, $J = 7.9$ Hz, 1H), 7.58 (s, 1H), 7.78 (dd, $J = 7.6$ and 7.3 Hz,1H), 8.04 (d, $J = 7.3$ Hz, 1H), 8.48 (br, 1H). IR: $\nu_{C=O}$, 1660 cm^{-1}.

2-[((2-(4-(*N*-Triphenylmethyl)imidazolyl)ethyl)amino)carbonyl]-6-[((2-amino-1,1,2-trimethylpropyl)amino)methyl]pyridine (3). A solution of **1** (12.81 g, 26.09 mmol) and 2,3-dimethylbutane-2,3-diamine (14.31 g, 123.4 mmol) in 150 mL of THF was heated at reflux for 8 days and concentrated in vacuo. The residue was purified by chromatography on silica gel (eluent, 20:1:0.1 → 10:1:0.1 CH_2Cl_2/CH_3OH/28% aqueous NH_3) to yield **3** as colorless needles (8.17 g, 53% based on **1**). ^1H NMR ($CDCl_3$): δ 1.06 (s, 6H), 1.14 (s, 6H), 1.64 (br, 3H), 2.87 (t, $J = 6.9$ Hz, 2H), 3.75 (q, $J = 6.9$ Hz, 2H), 3.89 (s, 2H), 6.62 (s, 1H), 7.10−7.27 (m, 15H), 7.38 (s, 1H), 7.55 (d, $J = 6.9$ Hz, 1H), 7.78 (dd, $J = 7.6$ and 6.9 Hz, 1H), 8.03 (d, $J = 7.6$ Hz, 1H), 8.53 (br, 1H).

2-[((2-(4-Imidazolyl)ethyl)amino)carbonyl]-6-[((2-amino-1,2,2-trimethylpropyl)amino)methyl]pyridine (L_4). To a solution of **3** (8.17 g, 13.92 mmol) in 60 mL of CH_3OH was added 3 mL of concentrated HCl dropwise. The solution was heated at reflux for 4 h and then concentrated in vacuo. The residue was dissolved in 0.5 M HCl (5 mL) and washed with CH_2Cl_2. The aqueous layer was evaporated to dryness. The residue was neutralized by anion-exchange resin, and the eluant was evaporated to yield $\mathbf{L_4}$ as a yellow oil (2.57 g, 54%). ^1H NMR ($CDCl_3$): δ 1.11 (s, 6H), 1.17 (s, 6H), 2.94 (t, $J = 6.6$ Hz, 2H), 3.14 (br, 3H), 3.75 (t, $J = 6.6$ Hz, 2H), 3.91 (s, 2H), 6.83 (s, 1H), 7.48 (d, $J = 7.9$ Hz, 1H), 7.55 (s, 1H), 7.78 (dd, $J = 7.9$ and 7.6 Hz, 1H), 8.03 (d, $J = 7.6$ Hz, 1H), 8.42 (br, 1H). IR: $\nu_{C=O}$, 1663 cm^{-1}.

Preparation of Copper(II) Complexes. $[Cu^{II}(H_{-1}L_3)]ClO_4$ (5·ClO_4), Method A. To a solution of $\mathbf{L_3}$ (30 mg, 0.09 mmol) in methanol (1 mL) was added dropwise a methanolic solution (1 mL) of $Cu(ClO_4)_2 \cdot 6H_2O$ (35 mg, 0.09 mmol) at room temperature. 1-Methylimidazole (30 mg, 0.37 mmol) was added to the solution, and the resulting blue solution was evaporated to dryness at 30 °C. Methanol (3 mL) was added to dissolve the residue. The solution was allowed to stand for a month, and the resulting blue crystals of **5**·ClO_4 were collected (22 mg, 49%). IR: $\nu_{C=O}$, 1575 cm^{-1}. Anal. Calcd (found) for $C_{16}H_{23}N_6O \cdot Cu(ClO_4)$: C, 40.17 (40.44); H, 4.85 (4.88); N, 17.57 (17.84).

5·ClO_4·1.5H_2O, Method B. A solution of $\mathbf{L_3}$ (16 mg, 0.05 mmol) and $Cu(ClO_4)_2 \cdot 6H_2O$ (19 mg, 0.05 mmol) in 30 mL of water was adjusted to pH 9.0 with 0.1 M aqueous NaOH. The mixture was filtered, and the filtrate was allowed to stand for 2 weeks at room temperature. Blue microcrystalline **5**·$ClO_4 \cdot 1.5H_2O$ was obtained in 49% yield. Anal. Calcd (found) for $C_{16}H_{23}N_6O \cdot Cu(ClO_4) \cdot 1.5H_2O$: C, 38.02 (37.85); H, 5.18 (4.79); N, 16.63 (16.23).

$[Cu^{II}(H_{-1}L_4)]BF_4 \cdot 0.5H_2O$ (7·BF_4·0.5H_2O). To a solution of $\mathbf{L_4}$ (174 mg, 0.051 mmol) in methanol (10 mL) was slowly added a solution of $Cu(OAc)_2 \cdot H_2O$ (100 mg, 0.50 mmol) in methanol (30 mL), and the mixture was stirred for 3 h at room temperature. A methanolic solution (4 mL) of $NaBF_4$ (55 mg, 0.50 mmol) was added, and the resulting mixture was kept at room temperature. Light blue blocks were deposited within 24 h and were collected by filtration, washed with methanol, and dried in vacuo. Recrystallization from a pH 9 aqueous solution afforded light blue crystals of **7**·$BF_4 \cdot 0.5H_2O$ in yield of 53% (135 mg). IR: $\nu_{C=O}$, 1575 cm^{-1}. Anal. Calcd (found) for $C_{18}H_{27}N_6O \cdot Cu(BF_4) \cdot 0.5H_2O$: C, 43.00 (43.08); H, 5.61 (5.52); N, 16.71 (16.45).

$[Cu^{II}(H_{-1}L_4)]ClO_4 \cdot 0.5H_2O$ (7·ClO_4·0.5H_2O). A procedure similar to that of the method B was employed using 0.061 mmol of $Cu(ClO_4)_2 \cdot 6H_2O$ and $\mathbf{L_4}$ to yield blue microcrystalline **7**·$ClO_4 \cdot 0.5H_2O$. Yield, 10 mg (32%). IR: $\nu_{C=O}$, 1575 cm^{-1}. Anal. Calcd (found) for $C_{18}H_{27}N_6O \cdot Cu(ClO_4) \cdot 0.5H_2O$: C, 41.94 (41.77); H, 5.48 (5.39); N, 16.30 (15.88).

$[Zn^{II}(L_3)](ClO_4)_2 \cdot H_2O$ (11·$(ClO_4)_2$·H_2O). A solution of $\mathbf{L_3}$ (100 mg, 0.316 mmol) and $Zn(ClO_4)_2 \cdot 6H_2O$ (118 mg, 0.316 mmol) in 15 mL of water was adjusted to pH 6.0 with 0.1 M aqueous HCl. The mixture was allowed to stand for 10 days at room temperature. Colorless microcrystalline **11**·$ClO_4 \cdot H_2O$ was obtained in 57% yield (108 mg). IR: $\nu_{C=O}$, 1642 cm^{-1}. Anal. Calcd (found) for $C_{16}H_{24}N_6O \cdot Zn(ClO_4)_2 \cdot H_2O$: C, 32.10 (31.76); H, 4.38 (4.20); N, 14.04 (13.66).

$[Zn^{II}(H_{-1}L_3)]ClO_4 \cdot H_2O$ (12·ClO_4·H_2O). A solution of **11**·$ClO_4 \cdot H_2O$ (100 mg, 0.167 mmol) in 10 mL of water was adjusted to pH 9.8 with 0.1 M aqueous NaOH. The mixture was filtered, and the filtrate was allowed to stand for 4 days at room temperature. Colorless microcrystalline **12**·$ClO_4 \cdot H_2O$ was obtained 18% yield (15 mg). IR: $\nu_{C=O}$, 1569 cm^{-1}. Anal. Calcd (found) for $C_{16}H_{23}N_6O \cdot Zn(ClO_4) \cdot H_2O$: C, 38.57 (38.31); H, 5.06 (5.03); N, 16.87 (16.46).

Caution! Perchlorate salts of metal complexes with organic ligands are potentially explosive. Only small amounts of material should be prepared, and these should be handled with care.

Crystallographic Studies. A blue crystal of $[Cu^{II}(H_{-1}L_3)]ClO_4$, **5**·$ClO_4$, (0.20 × 0.20 × 0.30 mm) and a light blue crystal of $[Cu^{II}(H_{-1}L_4)]BF_4$, **7**·BF_4 (0.30 × 0.06 × 0.03 mm), were selected and mounted on a glass fiber. All measurements were performed with a Rigaku AFC 7R diffractometer with graphite-monochromated Mo Kα radiation for **5**·ClO_4 and with graphite-monochromated Cu Kα radiation for **7**·BF_4. Cell constants and orientation matrixes were obtained from a least-squares refinement, using 25 reflections in the range $32.98° < 2\theta < 35.76°$ for **5**·ClO_4 and $52.38° < 2\theta < 56.41°$ for **7**·BF_4. Data were collected with the $\omega-2\theta$ scan technique. The intensities of three reflections were monitored in every 150 reflections, and no decay was observed. The data were corrected for Lorenz and polarization effects.

All the calculations were performed with the teXsan crystallographic software package (Molecular Structure Corp.) on an Iris Indigo workstation of Silicon Graphic Institutes.[20] The structures were solved by the direct method, and all the non-hydrogen atoms were located by Fourier methods and refined by full-matrix least squares. The scattering factors were taken from ref 21. For **5**·ClO_4, non-hydrogen atoms were refined anisotropically. All the hydrogen atoms were located from the final difference Fourier map but were not refined. For **7**·BF_4, non-hydrogen atoms were refined anisotropically, and all the hydrogen atoms were included in the models at their calculated positions but were not refined. Crystallographic data are presented in Table 1. Atomic positional parameters are given in Tables 2 and 3 for **5**·ClO_4 and **7**·BF_4, respectively. Additional material available from the Cambridge

(19) Sayre, R. *J. Am. Chem. Soc.* **1955**, *77*, 6689.

(20) teXsan: Crystal Structure Analysis Package. Molecular Structure Corporation (1985 & 1992).

(21) Cromer D. T.; Waber, J. T. *International Tables for X-ray Crystallography*; Kynoch Press: Birmingham, 1974; Vol. 4.

Table 1. Crystallographic Data for $[Cu^{II}(H_{-1}L_3)]ClO_4$, **5**·$ClO_4$, and $[Cu^{II}(H_{-1}\ L_4)]BF_4$, **7**·$BF_4$

	5·ClO_4	**7**·BF_4
formula	$CuC_{16}H_{23}N_6O_5Cl$	$CuC_{18}H_{27}N_6OBF_4$
fw	478.39	493.80
cryst color, habit	blue, prismatic	blue, prismatic
a, Å	13.978(6)	16.092(2)
b, Å	8.103(3)	7.974(4)
c, Å	18.037(5)	16.819(2)
β, deg	98.61(3)	99.64(1)
Z	4	4
cryst syst	monoclinic	monoclinic
space group	$P2_1/n$ (No. 14)	$P2_1/n$ (No. 14)
V, Å^3	2019(1)	2127(1)
T, °C	20 ± 1	20 ± 1
λ, Å	0.71069 (Mo Kα)	1.54178 (Cu Kα)
ρ_{cald}, g cm^{-3}	1.573	1.541
F(000)	988.00	1020.00
abs coeff (μ), cm^{-1}	12.55	19.70
R^a	0.053	0.040
$R_w{}^b$	0.044	0.025

^{a} $R = \sum||F_o| - |F_c||/\sum|F_o|$. ^{b} $R = [\sum w(|F_o| - |F_c|)^2/\sum w|F_o|^2]^{1/2}$, $w = (\sigma^2(F_o))^{-1}$.

Table 2. Positional Parameters and B_{eq} (Å^2) for $[Cu^{II}(H_{-1}L_3)]ClO_4$, **5**·$ClO_4$

atom	*x*	*y*	*z*	B_{eq}
Cu(1)	0.16711(5)	0.08873(8)	−0.03854(3)	2.93(1)
Cl(1)	0.0623(1)	0.3258(2)	0.33916(9)	4.88(4)
O(1)	0.1137(3)	−0.4023(4)	−0.0339(2)	4.11(9)
O(2)	0.1275(4)	0.3600(8)	0.4031(3)	11.1(2)
O(3)	0.0941(4)	0.3880(7)	0.2746(3)	8.2(2)
O(4)	0.0499(4)	0.1522(6)	0.3331(3)	8.9(2)
O(5)	−0.0298(3)	0.3995(6)	0.3452(2)	5.0(1)
N(1)	0.1333(3)	0.1847(5)	−0.1404(2)	3.1(1)
N(2)	0.0776(3)	0.3321(6)	−0.2388(2)	4.2(1)
N(3)	0.1440(3)	−0.1424(5)	−0.0749(2)	2.21(10)
N(4)	0.1379(3)	−0.0148(5)	0.0528(2)	1.98(10)
N(5)	0.1864(3)	0.2926(5)	0.0367(2)	2.39(10)
N(6)	0.3276(3)	0.1165(5)	−0.0288(2)	3.5(1)
C(1)	0.0951(4)	0.3287(6)	−0.1636(3)	3.4(1)
C(2)	0.1063(4)	0.1842(7)	−0.2649(3)	4.1(1)
C(3)	0.1416(4)	0.0923(7)	−0.2041(3)	3.3(1)
C(4)	0.1857(4)	−0.0752(7)	−0.1994(3)	4.1(1)
C(5)	0.1390(4)	−0.1990(6)	−0.1520(3)	3.8(1)
C(6)	0.1301(4)	−0.2502(6)	−0.0238(3)	2.6(1)
C(7)	0.1330(4)	−0.1777(6)	0.0522(3)	2.2(1)
C(8)	0.1282(4)	−0.2631(7)	0.1168(3)	4.0(1)
C(9)	0.1282(5)	−0.1746(8)	0.1833(3)	4.6(2)
C(10)	0.1307(4)	−0.0034(7)	0.1821(3)	4.3(2)
C(11)	0.1349(4)	0.0735(7)	0.1134(3)	3.1(1)
C(12)	0.1335(4)	0.2572(7)	0.0989(3)	3.9(1)
C(13)	0.2899(4)	0.3067(7)	0.0651(3)	3.4(1)
C(14)	0.3534(4)	0.2812(7)	0.0066(3)	3.6(1)
C(15)	0.4588(4)	0.2843(8)	0.0427(3)	5.6(2)
C(16)	0.3359(4)	0.4137(7)	−0.0543(3)	4.4(1)

Crystallographic Data Centre comprises H-atom coordinates, thermal parameters, and remaining bond distances and angles.

Potentiometric pH Titrations. The protonation constants for ligands $\mathbf{L_3}$ and $\mathbf{L_4}$ and complexation constants of Cu^{II} complexes were determined by potentiometric pH titration of 50 mL samples. The ligand concentration was 1×10^{-3} M with the ratio of metal to ligand of 1:1. pH Values were read with a HORIBA F-7SII pH meter. The temperature was kept at 25.0 ± 0.1 °C, and the ionic strength was adjusted to 0.1 M with $NaNO_3$. All the solutions were carefully protected from air by a stream of humidified argon. The protonation constants K_n are defined as $[H_nL]/[H_{n-1}L][H^+]$, and the 1:1 complexation constants ($K_{Cu^{II}H_{-1}L}$) as $[Cu^{II}(H_{-1}L)][H^+]/[Cu^{II}][L]$. p$K_a$ (which is the $-\log K_n$) and $\log K_{Cu^{II}H_{-1}L}$ were calculated by the method described previously.[22]

(22) Kodama, M.; Kimura, E. *J. Chem. Soc., Dalton Trans.* **1979**, 326.

Table 3. Positional Parameters and B_{eq} (Å^2) for $[Cu^{II}(H_{-1}L_4)]BF_4$, **7**·BF_4

atom	*x*	*y*	*z*	B_{eq}
Cu	0.18095(6)	0.1175(1)	−0.03474(5)	2.57(2)
B(1)	1.0199(6)	0.326(1)	0.3581(6)	4.3(3)
F(1)	0.9972(3)	0.1671(5)	0.3388(3)	6.4(1)
F(2)	0.9519(3)	0.4149(6)	0.3782(2)	6.4(1)
F(3)	1.0840(3)	0.3303(6)	0.4218(3)	9.1(2)
F(4)	1.0428(3)	0.4048(6)	0.2922(3)	7.3(2)
O(1)	0.1054(2)	−0.3699(5)	−0.0409(2)	3.0(1)
N(1)	0.1592(3)	0.2140(6)	−0.1473(3)	2.4(1)
N(2)	0.0960(3)	0.3360(6)	−0.2575(3)	2.9(1)
N(3)	0.1603(3)	−0.1185(7)	−0.0748(3)	2.5(1)
N(4)	0.1165(3)	0.0332(6)	0.0442(3)	2.2(1)
N(5)	0.1847(3)	0.3291(6)	0.0401(3)	2.4(1)
N(6)	0.3157(3)	0.1401(7)	−0.0060(3)	2.9(1)
C(1)	0.1181(4)	0.3500(8)	−0.1769(4)	2.7(2)
C(2)	0.1257(4)	0.1848(8)	−0.2807(4)	2.9(2)
C(3)	0.1646(3)	0.1089(9)	−0.2127(3)	2.2(1)
C(4)	0.2110(4)	−0.0525(8)	−0.2018(4)	3.1(2)
C(5)	0.1736(4)	−0.1837(8)	−0.1517(4)	2.9(2)
C(6)	0.1242(4)	−0.2196(7)	−0.0288(4)	2.2(2)
C(7)	0.1010(3)	−0.1337(8)	0.0436(3)	2.3(1)
C(8)	0.0657(4)	−0.2027(8)	0.1036(4)	3.0(2)
C(9)	0.0455(4)	−0.0995(9)	0.1644(3)	2.9(2)
C(10)	0.0593(4)	0.0701(8)	0.1628(4)	3.0(2)
C(11)	0.0962(4)	0.1354(8)	0.1011(3)	2.4(1)
C(12)	0.1151(4)	0.3151(8)	0.0873(4)	2.7(2)
C(13)	0.2734(4)	0.3425(8)	0.0909(4)	2.9(2)
C(14)	0.3374(4)	0.3081(8)	0.0321(4)	3.1(2)
C(15)	0.2844(4)	0.2084(10)	0.1590(4)	4.2(2)
C(16)	0.2842(4)	0.5168(9)	0.1287(4)	4.3(2)
C(17)	0.4297(4)	0.3047(9)	0.0758(4)	4.4(2)
C(18)	0.3301(4)	0.4373(9)	−0.0351(4)	4.1(2)

Electrochemical Experiments. Cyclic voltammetry (CV) was performed with a BAS-50W electrochemical analyzer in DMF at 25 ± 0.1 °C, and the dissolved oxygen in solution was purged with argon. A three-electrode system was employed: glassy carbon, GC (1 mm diameter), Ag/AgCl (saturated KCl), and Pt plate as working, reference, and auxiliary electrodes, respectively.

Results and Discussion

Preparation of Ligands. The synthetic procedures for $\mathbf{L_3}$ and $\mathbf{L_4}$ are illustrated in Scheme 1. The compounds **2** and **3** were synthesized by the reaction of **1** with 2-methylpropane-1,2-diamine and 2,3-dimethylbutane-2,3-diamine, respectively, in THF. Removal of the trityl group of **2** and **3** by HCl/MeOH yielded $\mathbf{L_3}$·3HCl and $\mathbf{L_4}$·3HCl, followed by neutralization with Amberlite IRA-400 (OH^- form). The total yield was ca. 30% based on **1**. IR spectra (KBr pellets) of $\mathbf{L_3}$ and $\mathbf{L_4}$ showed strong amide C═O stretching bands at 1660 and 1663 cm^{-1}, respectively. Characterization of the compounds was accomplished using ^{1}H NMR spectroscopy.

Preparation of 5-Coordinate Copper(II) Complexes. The reaction of $\mathbf{L_3}$ with an equimolar amount of $Cu(ClO_4)_2$·$6H_2O$ in methanol yielded blue crystals of $[Cu^{II}(H_{-1}L_3)]ClO_4$, **5**·$ClO_4$, upon addition of 1-methylimidazole. The reaction of $\mathbf{L_4}$ with an equimolar amount of $Cu(OAc)_2$·H_2O in methanol gave $[Cu^{II}(H_{-1}L_4)]BF_4$, **7**·BF_4, by addition of $NaBF_4$. The reaction of $\mathbf{L_3}$ or $\mathbf{L_4}$ with $Cu(ClO_4)_2$·$6H_2O$ in water (adjusted to pH 9) gave also the corresponding copper(II) complexes described above. The IR spectra of these complexes showed bands at 1575 cm^{-1} lower by ca. 90 cm^{-1} than both of acid-free ligands, indicating a deprotonation of the amide group. The elemental analyses of all the copper(II) complexes were consistent with the composition of $[Cu^{II}(H_{-1}L)]X$ where $H_{-1}L$ denotes the deprotonated amide of the ligand and X = ClO_4 for $\mathbf{L_3}$ and X = ClO_4 or BF_4 for $\mathbf{L_4}$.

Scheme 1

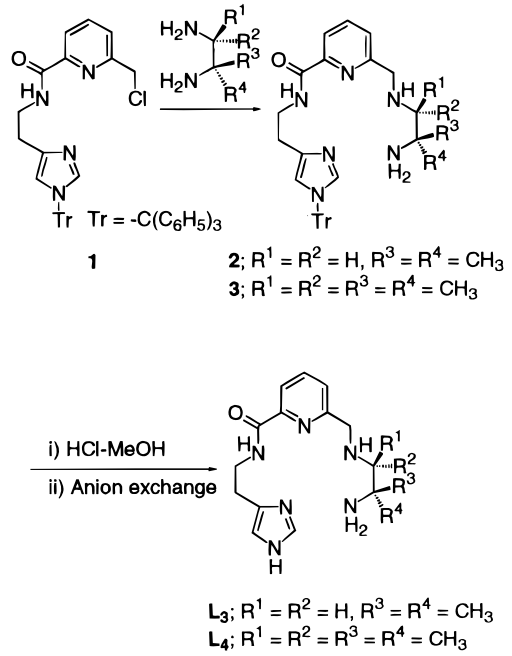

Table 4. Comparison of Protonation Constants and Complexation Constants of L_1, L_2, L_3, and L_4 with Cu^{II} at 25 °C and $I = 0.1$ M $NaNO_3$[c]

	L_1[a]	L_2[a]	L_3	L_4
log K_1	9.8	7.8	9.9	10.0
log K_2	7.3 (Im)[b]	6.9 (Im)[b]	6.9 (Im)[b]	6.7 (Im)[b]
log K_3	5.6	3.7	5.2	3.9
Cu^{II}, log $K_{Cu^{II}H_{-1}L}$	8.7	7.0	8.9	8.6[c]

[a] At 25 °C and $I = 0.2$ ($NaClO_4$) from ref 15. [b] Im = imidazole. [c] $K_{Cu^{II}H_{-1}L} = [Cu^{II}H_{-1}L][H^+]/[Cu^{II}][L]$.

Protonation and Copper(II) Complexation Constants for L_3 and L_4. The protonation constants (K_n) of L_3 and L_4 were determined by potentiometric pH titration of 1.0 mM L_3·3HCl and L_4·3HCl at 25 °C and $I = 0.10$ M $NaNO_3$. The titration curves of the ligand L_3 and L_4 are shown in Figures 1a and 2a, respectively. The titration data were analyzed for equilibria 1−3. The mixed protonation constants K_1-K_3 are defined as follows.

$$L + H^+ \rightleftharpoons HL \qquad K_1 = [HL]/[L][H^+] \qquad (1)$$

$$HL + H^+ \rightleftharpoons H_2L \qquad K_2 = [H_2L]/[HL][H^+] \qquad (2)$$

$$H_2L + H^+ \rightleftharpoons H_3L \qquad K_3 = [H_3L]/[H_2L][H^+] \qquad (3)$$

The obtained protonation constants (log K_n) are listed in Table 4 and compared with K_n values for L_1[15] and L_2.[15] For L_3·3HCl, the inflection occurred at $a = 2$, while the inflections occurred at $a = 1$ and 2 for L_4·3HCl. The computed log K_n values were 9.9, 6.9, and 5.2 for L_3 and 10.0, 6.7, and 3.9 for L_4. The log K_1 and log K_2 values were almost the same as those for unsubstituted L_1;[15] however, the log K_3 for L_4 was smaller than those for L_1[15] and L_3 due to the substituent effect of two methyl groups adjacent to the secondary amine group. The substituent effect of the lowering on acidity closely parallels those on the observed acidities of 1,2-ethanediamine (7.6 and 10.7), 2-methylpropane-1,2-diamine (6.5, 10.1), and 2,3-dimethylbutane-2,3-diamine (6.0 and 10.2).[23]

Scheme 2

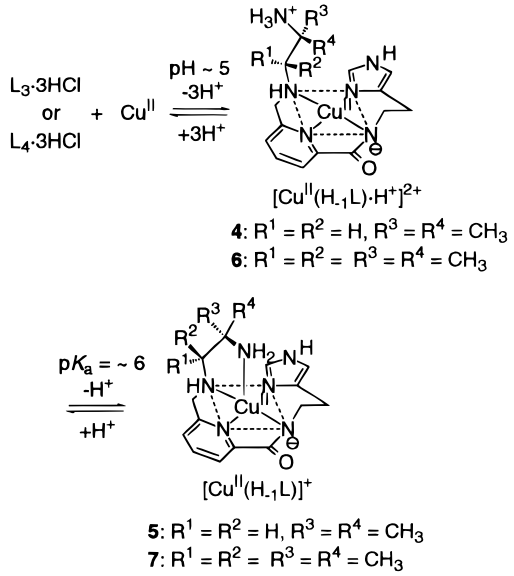

The binding constants for the binding of Cu^{II} with L_3 and L_4 were determined by potentiometric pH titration of the triprotonated L_3·$3H^+$ or L_4·$3H^+$ (1 mM) in the presence of an equimolar amount of Cu^{II} at 25 °C and $I = 0.10$ M $NaNO_3$. For the triprotonated L_3 and L_4, the smooth buffer curves ($0 < a < 3$) shown in Figures 1b and 2b indicate the neutralization of the ligand accompanied with Cu^{II} complexation to form 4-coordinate $[Cu^{II}(H_{-1}L)\cdot H^+]^{2+}$ complexes, **4** and **6**. In this buffer region, $H_{-1}L\cdot H^+$ stands for the species in which the deprotonated amide is coordinated while the primary amine kept protonated and uncoordinated. Analogous species has been reported for Cu^{II} complex of L_1, $[Cu^{II}(H_{-1}L_1)\cdot H^+]^{2+}$, **8**, which was isolated as perchlorate salts.[15b] In the second buffer region at $3 < a < 4$, the loss of one proton from the primary amine yields 5-coordinate $[Cu^{II}H_{-1}L]^+$ complexes, **5** and **7**, with pK_a values of ~ 6 (see Scheme 2). These final products were isolated from the pH-titration solutions as blue prisms of $[Cu^{II}(H_{-1}L_3)]$-$ClO_4\cdot 1.5H_2O$ (**5**·$ClO_4\cdot 1.5H_2O$) and $[Cu^{II}(H_{-1}L_4)]ClO_4\cdot 0.5H_2O$ (**7**·$ClO_4\cdot 0.5H_2O$). Their IR spectra and elemental analysis (C, H, N) agreed with those of the copper(II) complexes isolated from a solution of L_3 or L_4 in the presence of an equimolar amount of $Cu(ClO_4)_2\cdot 6H_2O$ in water at pH 9.0.

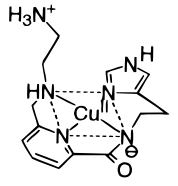

From the analysis of the titration data at $a < 4$, the Cu^{II} complexation constants ($K_{Cu^{II}H_{-1}L} = [Cu^{II}(H_{-1}L)][H^+]/[Cu^{II}][L]$) for L_3 and L_4, log $K_{Cu^{II}H_{-1}L} = 8.9$ for L_3 and 8.6 for L_4, were determined (Table 4). The log $K_{Cu^{II}H_{-1}L}$ values for L_3 and L_4 are almost the same as that for L_1.[15]

Interaction of Cu^I−L_3 and −L_4. Titrations for 1:1 Cu^I (from $Cu^I(CH_3CN)_4ClO_4$)−L_3 or −L_4 were performed in a 5% CH_3-

(23) The protonation constants (K_n) for diamines were determined by a potentiometric pH-titration of the corresponding diamine dihydrochloride salts (5 mM) with $I = 0.10$ M $NaNO_3$ at 25 °C.

Scheme 3

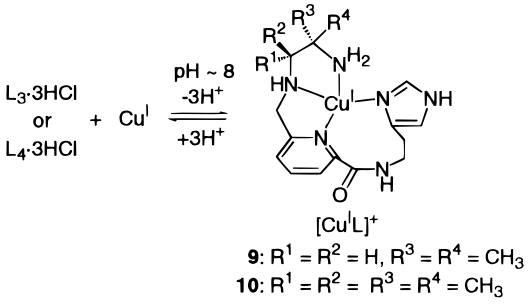

Scheme 4

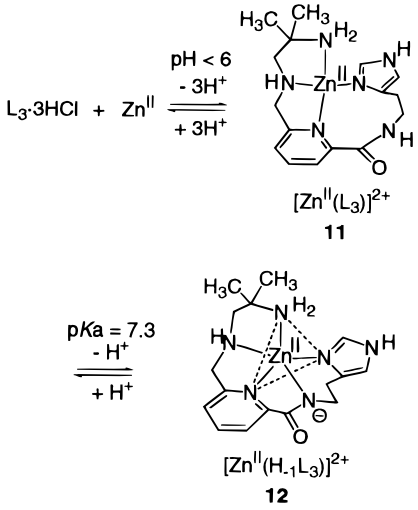

CN aqueous solution. The titration curves shown in Figures 1c and 2c showed no break at $a(OH^-) = 3$, being quite different from those of the corresponding Cu^{II} complexes $Cu^{II}-L_3$ and L_4 ($a(OH^-) = 4$). These results suggest that formation of 4-coordinate Cu^I complexes with un-deprotonated amides, **9** and **10** (see Scheme 3). To substantiate this claim, the isoelectronic Zn^{II} complexes were employed for the pH titration with L_3 and L_4. The titration curves with L_3 and L_4, shown in Figures 1e and 2e, showed two inflections at $a(OH^-) = 3$ and 4 as those for Cu^{II}. In L_3, colorless crystals were separated from the titration solution at pH ~ 6 (i.e., $a(OH^-) = 3$), which are different from the crystals isolated from the medium of pH 9 ($a(OH^-) = 4$) of which the crystal study showed that the Zn^{II} center has the trigonal-bipyramidal structure, **12**.[18] Because the former crystals showed an amide $\nu_{C=O}$ of 1642 cm^{-1} and the microanalysis agreed with the formula $[Zn^{II}L_3](ClO_4)\cdot H_2O$, the Zn^{II} complex should have the tetrahedral 4-coordinated structure, **11** (see Scheme 4). These findings strongly support the formation of a tetrahedral Cu^I complex with L_3 or L_4 since Cu^I and Zn^{II} are isoelectronic and the less positive charge of Cu^I should decrease the ability for the deprotonation of the amide.

After O_2-bubbling oxidation of **9** and **10**, their UV−visible spectra in 5% CH_3CN aqueous solution are identical to those of the corresponding 5-coordinate Cu^{II} complexes, **5** and **7**.

pH Titration of Fe^{II} with L_3 and L_4. Moreover, we have investigated the pH titrations of L_3 or L_4 with Fe^{II} at 25 °C and $I = 0.1$ M $NaNO_3$ (see Figures 1d and 2d). It is remakable that their complexation reactions are quite different from that of the $Fe^{II}-L_1$ complex. Interaction of L_1 with Fe^{II} is so weak that the complex does not survive above neutral pH,[15] while L_3 and L_4 could form stable Fe^{II} complexes even at pH 10. The titration curve for L_3 with Fe^{II} shows one inflection at $a(OH^-) = 4$, indicating that loss of the four protons is required to form a

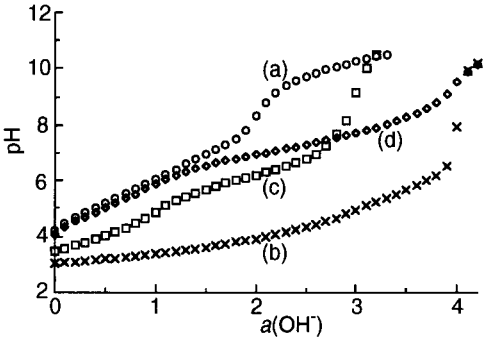

Figure 1. pH Titration curves of triprotonated ligands H_3L_3 in the absence and the presence of equimolar Cu^{II}, Cu^I, or Fe^{II} at 25 °C and $I = 0.1$ M $NaNO_3$. Key: (a) 1.0 mM L_3·3HCl; (b) (a) + 1.0 mM $CuSO_4\cdot 6H_2O$; (c) (a) + 1.0 mM $Cu(CH_3CN)_4\cdot ClO_4$; (d) (a) + 1.0 mM $FeSO_4\cdot 7H_2O$; (e) (a) + 1.0 mM $Zn(NO_3)_2\cdot 6H_2O$.

Scheme 5

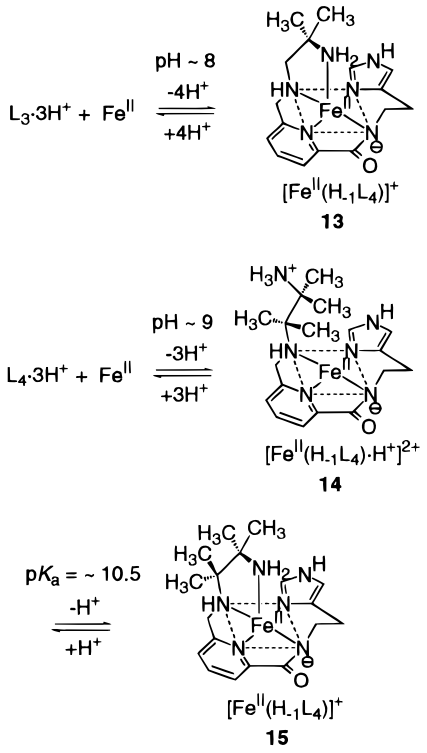

stable $[Fe^{II}(H_{-1}L_3)]^+$, (**13**), as shown in Scheme 5, which is analogous to the 5-coordinate $Fe^{II}-L_2$ complex.[15] In $Fe^{II}-L_4$, the titration curve shows two inflections at $a(OH^-) = 1$ and 4. The first buffer region (pH < 7) until $a = 3$ is ascribed to the loss of the three protons to form a 4-coordinate $[Fe^{II}(H_{-1}L_4)\cdot H^+]^{2+}$ (**14**). The second buffer region at $3 < a < 4$ represents the removal of one proton to form the 5-coordinate $[Fe^{II}(H_{-1}L_4)]^+$ (**15**) with a pK_a value of 10.3. These results show the introduction of two or four methyl groups to the carbon atoms of the ligand significantly stabilizes the Fe^{II} complexes at physiological pH.

Description of the Structures. Crystal Structure of $[Cu^{II}(H_{-1}L_3)]ClO_4$ (5·ClO_4). The blue crystals suitable for X-ray diffraction study were obtained by slow evaporation of a methanolic solution. The crystal structure of **5**·ClO_4 consists of discrete five-coordinate $[Cu^{II}(H_{-1}L_3)]^+$, **5**, and a perchlorate ion. The ORTEP drawing of the cationic part is shown in Figure 3, and bond distances and angles are listed in Table 5. The coordination geometry around the central Cu(II) atom is a

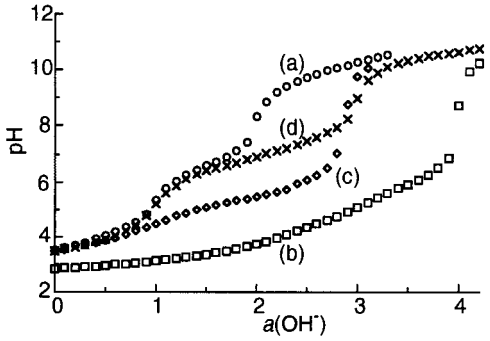

Figure 2. pH Titration curves of triprotonated ligands H_4L_4 in the absence and the presence of equimolar Cu^{II}, Cu^{I}, or Fe^{II} at 25 °C and I = 0.1 M $NaNO_3$. Key: (a) 1.0 mM L_4·3HCl; (b) (a) + 1.0 mM $CuSO_4$·$6H_2O$; (c) (a) + 1.0 mM $Cu(CH_3CN)_4$·ClO_4; (d) (a) + 1.0 mM $FeSO_4$·$7H_2O$; (e) (a) + 1.0 mM $Zn(NO_3)_2$·$6H_2O$.

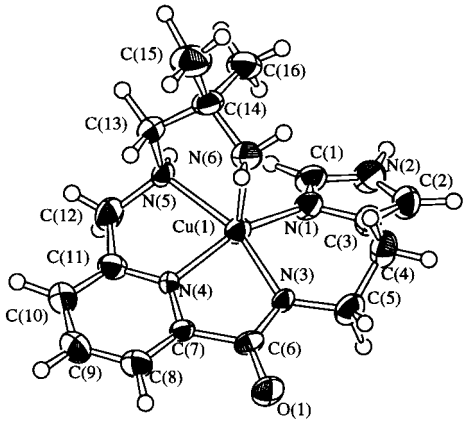

Figure 3. ORTEP diagram of $[Cu^{II}(H_{-1}L_3)]^+$, **5**, illustrating the numbering scheme. The thermal ellipsoids are drawn at the 50% level.

distorted square pyramidal with τ[24] = 0.087 (α = 154.3(2)° and β = 159.5(2)°). Four nitrogens from the imidazoyl N(1), deprotonated amide N(3), pyridyl N(4), and the secondary amine N(5) make the basal plane with the terminal primary amine N(6), occupying the apical position. The N(1), N(3), N(4), and N(5) atoms lie −0.149(4), 0.206(4), −0.218(4), and 0.185(4) Å, respectively, out of the least-squares plane through them; the Cu atom is displaced 0.242 Å above the mean basal plane to the direction of the axial N(6) atom. The largest deviation from the ideal geometry is manifested in the N(1)−Cu−N(4) angles of 154.3(2)°, which reflects the N(4)−Cu−N(6) bite angle of 108.2(2)°.

The Cu−N(1) (imidazole) and Cu−N(3) (amide) distances for **5** are 1.986(4) and 1.994(4) Å, respectively, and are within

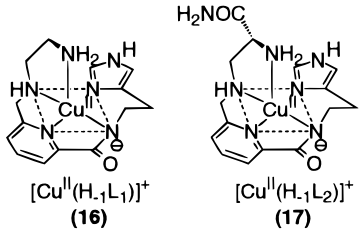

the range noted for $[Cu^{II}(H_{-1}L_2)]^+$, **17** (1.953(3) and 1.993(3) Å),[15b] and for copper(II) complexes of glycine-L-histidine[25] and glycyl-L-histidylglycine[26] (1.93−1.98 and 1.93−1.99 Å, respectively). The Cu−N(4) (pyridine) bond distance of 1.946(4) Å for **5** is similar to that of **17** (1.930(3) Å).[15b] The Cu−N(5) (secondary amine) distance of 2.130(4) Å for **5** is also close to that of 2.099(3) Å for **17**.[15b] The axial Cu−N(6) (primary amine) bond distance of 2.235(4) Å is a little shorter than that of 2.319(3) Å for **17**.[15b] The difference is probably due to the stronger amine basicity for **5** than that for **17**.[15b]

The pyridyl and imidazoyl rings are planar (rms deviations 0.0094 and 0.0031 Å, respectively). The dihedral angle of the pyridyl and imidazoyl rings is 26.62° and is a little smaller than those of 33.68° for **17**.[15b]

The amine hydrogens show close contacts to the oxygen atoms of the perchlorate ion, indicating hydrogen bonds (N(2)−H(2)···O(5), 1.85 Å, N(5)−H(21)···O(1), 1.97 Å, and N(6)−H(23)···O(5), 2.28 Å). The oxygen atom O(1) of the amide group is also hydrogen bonded to the hydrogen atom of N(5) of a neighboring complex cation: N(5)−H(21)···O(1), 2.31 Å.

Crystal Structure of $[Cu^{II}(H_{-1}L_4)]BF_4$ (7·BF_4). The blue crystals suitable for X-ray diffraction study were obtained by slow evaporation of a pH 9 aqueous solution. The crystal structure of **7**·BF_4 consists of discrete five-coordinate $[Cu^{II}(H_{-1}L_4)]^+$, **7**, and a tetrafluoroborate ion. The ORTEP

Table 5. Selected Bond Distances (Å) and Angles (deg) for $[Cu^{II}(H_{-1}L_3)]ClO_4$, **5**·$ClO_4$

bond distances			
Cu(1)−N(1)	1.986(4)	Cu(1)−N(3)	1.994(4)
Cu(1)−N(4)	1.946(4)	Cu(1)−N(5)	2.130(4)
Cu(1)−N(6)	2.235(4)	O(1)−C(6)	1.262(6)
N(1)−C(1)	1.324(6)	N(1)−C(3)	1.390(6)
N(2)−C(1)	1.342(6)	N(2)−C(2)	1.370(7)
N(3)−C(5)	1.456(6)	N(3)−C(6)	1.305(6)
N(4)−C(7)	1.322(6)	N(4)−C(11)	1.313(6)
N(5)−C(12)	1.461(6)	N(5)−C(13)	1.465(7)
N(6)−C(14)	1.500(7)	C(2)−C(3)	1.355(7)
C(3)−C(4)	1.488(7)	C(4)−C(5)	1.528(7)
C(6)−C(7)	1.485(7)	C(7)−C(8)	1.366(7)
C(8)−C(9)	1.397(7)	C(9)−C(10)	1.388(7)
C(10)−C(11)	1.396(7)	C(11)−C(12)	1.511(7)
C(13)−C(14)	1.492(7)	C(14)−C(15)	1.519(7)
C(14)−C(16)	1.530(7)		

bond angles			
N(1)−Cu(1)−N(3)	93.4(2)	N(1)−Cu(1)−N(4)	154.3(2)
N(1)−Cu(1)−N(5)	106.0(2)	N(1)−Cu(1)−N(6)	97.5(2)
N(3)−Cu(1)−N(4)	80.2(2)	N(3)−Cu(1)−N(5)	159.5(2)
N(3)−Cu(1)−N(6)	103.4(2)	N(4)−Cu(1)−N(5)	79.5(2)
N(4)−Cu(1)−N(6)	108.2(2)	N(5)−Cu(1)−N(6)	80.9(2)
Cu(1)−N(1)−C(1)	131.7(4)	Cu(1)−N(1)−C(3)	121.0(3)
C(1)−N(1)−C(3)	107.1(4)	C(1)−N(2)−C(2)	108.1(5)
Cu(1)−N(3)−C(5)	126.3(3)	Cu(1)−N(3)−C(6)	115.5(3)
C(5)−N(3)−C(6)	118.2(4)	Cu(1)−N(4)−C(7)	116.1(4)
Cu(1)−N(4)−C(11)	120.5(4)	C(7)−N(4)−C(11)	122.9(5)
Cu(1)−N(5)−C(12)	107.8(3)	Cu(1)−N(5)−C(13)	107.9(3)
C(12)−N(5)−C(13)	109.4(4)	Cu(1)−N(6)−C(14)	107.4(3)
N(1)−C(1)−N(2)	109.9(5)	N(2)−C(2)−C(3)	107.1(5)
N(1)−C(3)−C(2)	107.9(5)	N(1)−C(3)−C(4)	122.0(4)
C(2)−C(3)−C(4)	130.1(5)	C(3)−C(4)−C(5)	115.0(5)
N(3)−C(5)−C(4)	111.4(4)	O(1)−C(6)−N(3)	126.5(5)
O(1)−C(6)−C(7)	119.9(5)	N(3)−C(6)−C(7)	113.6(4)
N(4)−C(7)−C(6)	113.4(5)	N(4)−C(7)−C(8)	120.5(5)
C(6)−C(7)−C(8)	126.1(5)	C(7)−C(8)−C(9)	118.6(5)
C(8)−C(9)−C(10)	119.8(6)	C(9)−C(10)−C(11)	117.7(6)
N(4)−C(11)−C(10)	120.5(5)	N(4)−C(11)−C(12)	113.1(5)
C(10)−C(11)−C(12)	126.4(5)	N(5)−C(12)−C(11)	109.4(4)
N(5)−C(13)−C(14)	113.7(4)	N(6)−C(14)−C(13)	107.1(4)
N(6)−C(14)−C(15)	110.7(5)	N(6)−C(14)−C(16)	108.4(4)
C(13)−C(14)−C(15)	109.6(5)	C(13)−C(14)−C(16)	111.3(5)
C(15)−C(14)−C(16)	109.7(5)		

(24) Addison, A. W.; Rao, T. N.; Reedijk, J.; Rijn, J.; Verschoor, G. C. *J. Chem. Soc., Dalton Trans.* **1984**, 1349.
(25) Blount, J. F.; Fraser, K. A.; Freeman, H. C.; Szymanski, J. T.; Wang, C.-H. *Acta Crystallogr.* **1967**, *22*, 396.
(26) (a) de Meester, P.; Hodgson, D. J. *Acta Crystallogr.* **1977**, *B33*, 3505.

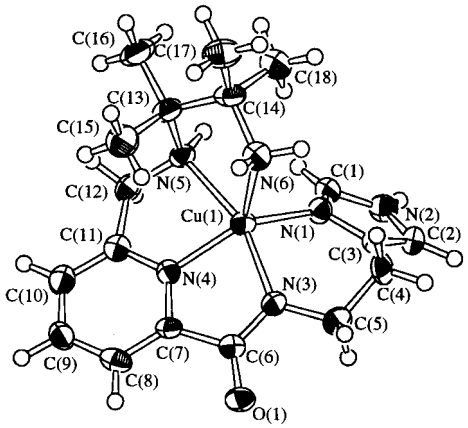

Figure 4. ORTEP diagram of $[Cu^{II}(H_{-1}L_4)]^+$, **7**, illustrating the numbering scheme. The thermal ellipsoids are drawn at the 50% level.

Table 6. Selected Bond Distances (Å) and Angles (deg) for $[Cu^{II}(H_{-1}L_4)]BF_4$, **7**·BF_4

bond distances			
Cu(1)−N(1)	2.019(5)	Cu(1)−N(3)	2.007(6)
Cu(1)−N(4)	1.937(5)	Cu(1)−N(5)	2.100(5)
Cu(1)−N(6)	2.149(4)	O(1)−C(6)	1.245(7)
N(1)−C(1)	1.323(7)	N(1)−C(3)	1.397(7)
N(2)−C(1)	1.346(7)	N(2)−C(2)	1.378(7)
N(3)−C(5)	1.443(7)	N(3)−C(6)	1.318(7)
N(4)−C(7)	1.353(8)	N(4)−C(11)	1.338(7)
N(5)−C(12)	1.482(7)	N(5)−C(13)	1.540(7)
N(6)−C(14)	1.500(8)	C(2)−C(3)	1.351(8)
C(3)−C(4)	1.484(8)	C(4)−C(5)	1.529(8)
C(6)−C(7)	1.496(8)	C(7)−C(8)	1.355(8)
C(8)−C(9)	1.394(8)	C(9)−C(10)	1.372(9)
C(10)−C(11)	1.381(8)	C(11)−C(12)	1.491(8)
C(13)−C(14)	1.567(8)	C(13)−C(15)	1.555(9)
C(13)−C(16)	1.526(9)	C(14)−C(17)	1.543(9)
C(14)−C(18)	1.520(8)		
bond angles			
N(1)−Cu(1)−N(3)	92.9(2)	N(1)−Cu(1)−N(4)	138.3(2)
N(1)−Cu(1)−N(5)	103.8(2)	N(1)−Cu(1)−N(6)	100.9(2)
N(3)−Cu(1)−N(4)	80.1(2)	N(3)−Cu(1)−N(5)	160.2(2)
N(3)−Cu(1)−N(6)	105.0(2)	N(4)−Cu(1)−N(5)	80.4(2)
N(4)−Cu(1)−N(6)	120.7(2)	N(5)−Cu(1)−N(6)	82.6(2)
Cu(1)−N(1)−C(1)	131.5(4)	Cu(1)−N(1)−C(3)	119.0(4)
C(1)−N(1)−C(3)	106.7(5)	C(1)−N(2)−C(2)	108.1(5)
Cu(1)−N(3)−C(5)	126.7(4)	Cu(1)−N(3)−C(6)	116.1(4)
C(5)−N(3)−C(6)	116.9(5)	Cu(1)−N(4)−C(7)	117.0(4)
Cu(1)−N(4)−C(11)	120.1(4)	C(7)−N(4)−C(11)	122.6(5)
Cu(1)−N(5)−C(12)	108.2(4)	Cu(1)−N(5)−C(13)	108.6(3)
C(12)−N(5)−C(13)	114.9(5)	Cu(1)−N(6)−C(14)	108.9(4)
N(1)−C(1)−N(2)	110.1(5)	N(2)−C(2)−C(3)	106.6(5)
N(1)−C(3)−C(2)	108.5(6)	N(1)−C(3)−C(4)	121.3(5)
C(2)−C(3)−C(4)	130.1(6)	C(3)−C(4)−C(5)	115.1(5)
N(3)−C(5)−C(4)	112.3(5)	O(1)−C(6)−N(3)	127.7(6)
O(1)−C(6)−C(7)	119.2(6)	N(3)−C(6)−C(7)	113.1(5)
N(4)−C(7)−C(6)	112.7(5)	N(4)−C(7)−C(8)	119.5(6)
C(6)−C(7)−C(8)	127.7(6)	C(7)−C(8)−C(9)	119.1(6)
C(8)−C(9)−C(10)	120.6(6)	C(9)−C(10)−C(11)	118.5(6)
N(4)−C(11)−C(10)	119.7(6)	N(4)−C(11)−C(12)	113.2(5)
C(10)−C(11)−C(12)	127.1(6)	N(5)−C(12)−C(11)	110.4(5)
N(5)−C(13)−C(14)	106.5(5)	N(5)−C(13)−C(15)	110.0(5)
N(5)−C(13)−C(16)	108.9(5)	C(14)−C(13)−C(15)	109.8(6)
C(14)−C(13)−C(16)	112.4(6)	C(15)−C(13)−C(16)	109.2(5)
N(6)−C(14)−C(13)	107.2(5)	N(6)−C(14)−C(17)	108.9(5)
N(6)−C(14)−C(18)	107.7(5)	C(13)−C(14)−C(17)	112.6(6)
C(13)−C(14)−C(18)	112.0(5)	C(17)−C(14)−C(18)	108.3(6)

drawing of the cationic part is shown in Figure 4, and selected bond distances and angles are listed in Table 6. The geometry around the copper center in **7**, however, is the intermediate between a square pyramid and a trigonal bipyramid with τ[24] = 0.37 (α = 138.3(2)° and β = 160.2(2)°).

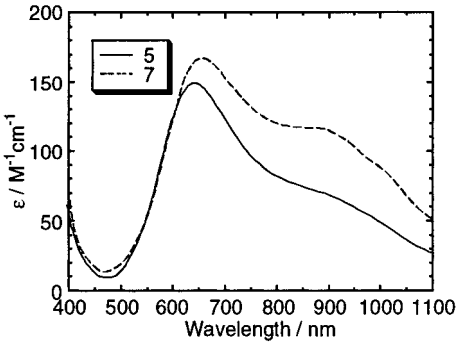

Figure 5. Electronic spectra of **5** (solid line) and **7** (broken line) in 10% DMF−water, containing I = 0.1 M ($NaNO_3$).

Table 7. Comparison of Visible and EPR Spectra for Cu^{II} Complexes

compound	visible[a] λ_{max}, nm (ϵ)	EPR (77 K)[b], $A_{\parallel}$/mT
$Cu^{II}(H_{-1}L_1)$ **(16)**[c]	600 (120)	17.9
$Cu^{II}(H_{-1}L_2)$ **(17)**[c]	595 (120)	17.9
$Cu^{II}(H_{-1}L_3)$ **(5)**	646 (149), 900sh (68)	16.5
$Cu^{II}(H_{-1}L_4)$ **(7)**	658 (166), 888 (116)	14.5
BLM[d]	595 (120)	18.3

[a] In H_2O (pH 9); ϵ in M^{-1} cm^{-1}. [c] From ref 15. [d] From ref 29.

The Cu−N(1), −N(3), −N(4), and −N(6) bond distances (average 2.016 Å) are close to those of $[Cu^{II}(H_{-1}L_3)]^+$ complex, **5** (average 2.014 Å), while the Cu−N(6) distance of 2.149(4) Å is slightly shorter than that of **5** (2.235(5) Å). The distortion from the ideal square-pyramidal geometry is much larger than in **7**, with the greatest deviation being the N(1)−Cu−N(4) of 138.3(2) °, which is due to the N(4)−Cu−N(6) angle of 120.7-(2) °, reflecting steric repulsion between the substituted methyl C(15) and the L_4 skeleton. The atoms forming the base plane, i.e. N(1), N(3), N(4), and N(5), deviate −0.240(5), 0.308(4), −0.390(5), and 0.273(5) °, respectively, from the least-squares plane through them, the Cu atom lying 0.380 Å above this plane to the direction of N(6) atom. The torsion angle of the pyridyl and imidazole ring is 51.97°. The torsion angle between the least-squares planes of two successive five-membered rings defined by Cu−N(4)−C(11)−C(12)−N(5) and Cu−N(5)−C(13)−C(14)−N(5) is 65.90°.

Thus, the introduction of the methyl group leads to distortion from a square pyramidal toward a trigonal bipyramidal geometry. There are several intermolecular contacts between the amine hydrogens and the fluorine atoms of the counterion: N(2)−H(2)···F(2), 1.93 Å; N(6)−H(26)···F(3), 2.24 Å; N(2)−H(2)···F(4), 2.21 Å. In analogy with **5**, the oxygen atom O(1) of the amide group is hydrogen bonded to a hydrogen atom of neighboring cations N(6): N(5)−H(13)···O(1), 2.05 Å.

Electronic Absorption Spectra. The absorption spectra of **5** and **7** in 10% DMF−water (pH 9.5) at I = 0.1 M $NaNO_3$ are shown in Figure 5 and the absorption maxima are summarized in Table 7 together with the data for the related compounds. The visible spectra for **5** and **7** exhibited absorption maxima λ_{max} at 646 nm (ϵ = 149) with a shoulder at ca. 900 nm (ϵ = 68) for **5** and at λ_{max} 658 nm (ϵ = 166) and 888 nm (ϵ = 116) for **7**, respectively. The absorption maxima at 646 and 658 nm and the shoulder bands around 900 nm are assigned to the d_{xz}, $d_{yz} \rightarrow d_{x^2-y^2}$ and the $d_{xy} \rightarrow d_{x^2-y^2}$ transitions, respectively, on the basis of the assignment of $K[Cu(NH_3)_5](PF_6)_3$,[27] which has a typical square-pyramid complex cation and exhibts only two

(27) Hathaway, B. J.; Tomlinson, A. A. *Coord. Chem. Rev.* **1970**, *5*, 30.

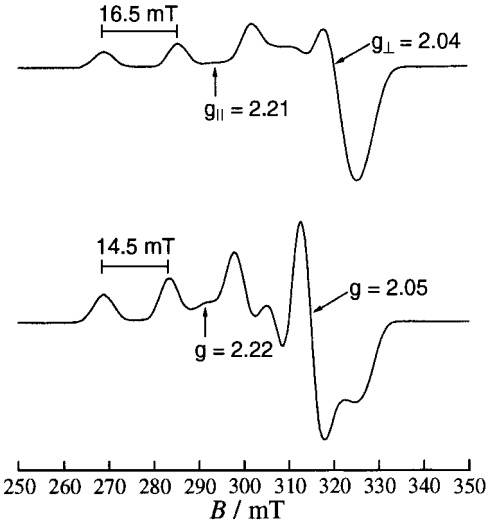

Figure 6. X-band EPR spectra (77 K) of **5** (top) and **7** (bottom) in DMF/MeOH (1:1 v/v).

bands at 667 and 877 nm. The spectral feature of five-coordinate copper(II) complexes with square-pyramidal or distorted square-pyramidal geometries generally is a band in the range of about 550−670 nm (allowed d_{xz}, $d_{yz} \rightarrow d_{x^2-y^2}$), while trigonal bipyramidal copper(II) complexes usually exhibit a maximum at >800 nm (d_{xy}, $d_{x^2-y^2} \rightarrow d_{z^2}$) with a higher energy shoulder (spin forbidden d_{xy}, $d_{x^2-y^2} \rightarrow d_{z^2}$).[28] The d−d transition bands for **5** and **7** were significantly shifted to longer wavelengths (ca. 50 nm) compared with those for the copper(II) complexes of BLM (λ_{max} 595 nm)[10b,29] and the synthetic analogues (λ_{max} 600 nm for $Cu^{II}-L_1$, **16**,[15] λ_{max} 595 nm for $Cu^{II}-L_2$, **17**,[15] see Table 7). The remarkable red shifts observed for **5** and **7** indicate a weak in-plane field strength compared with other Cu^{II} complexes. Moreover, the red shift of **7** by 12 nm compared to **5** suggested that its geometry is further distorted toward trigonal bipyramidal than that of **6** in solution. Thus, these spectral data of **5** and **7** are consistent with the degree of deviations found in their crystal structure.

EPR Studies. The EPR spectra of **5** and **7** in DMF/MeOH (1:1 v/v) at 77 K are shown in Figure 6. The EPR spectrum of **5** was typical to axially symmetric copper(II) complex with $g_{||} > g_\perp$ ($g_{||} = 2.21$, $g_\perp = 2.04$, $A_{||} = 16.5$ mT for **5**) and a $d_{x^2-y^2}$ ground-state doublet. On the other hand, the spectrum of **7** was different from that of **5** and displayed some rhombical distortions. The feature of the EPR spectra, common to the two series **5** and **7**, is the marked reduction in $A_{||}$ as the number of the methyl group increases. The smaller $A_{||}$ values suggest that **7** assumes a more distorted square-pyramidal structure than **5**. The lower $A_{||}$ values observed in **5** and **7** suggest the off-planar distortion is greater than the related Cu^{II} complexes.[30] These

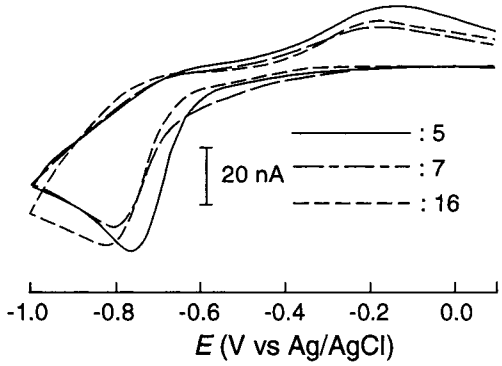

Figure 7. Cyclic voltammograms of 0.1 mM Cu^{II} complexes in DMF containing 0.1 M $TBABF_4$ on GC electrode ($S = (6 \pm 0.5) \times 10^{-3}$ cm^2) at 25 ± 1 °C. Scan rate = 50 mV s^{-1}.

results have been also confirmed by the crystal structures of complexes **5** and **7**.

Electrochemistry. The effects of introducing a methyl group are also reflected in the redox properties of the Cu^{II} complexes. The redox properties of compounds **5** and **7** have been studied by cyclic voltammetry in DMF at 25 °C and $I = 0.1$ M $TBABF_4$ as shown in Figure 7. A reduction wave was observed at $E_{pc} = -0.76$ for **5** and −0.80 V for **7** vs Ag/AgCl. The cathodic peak currents (i_{pa}) were proportional to the square root of the potential scan rates, υ ($20 < \upsilon < 200$ mV s^{-1}), for **5** or **7**, indicating a diffusion-controlled process with a diffusion coefficient (D) of $(2.5 \pm 1.0) \times 10^{-6}$ cm^2 s^{-1} by assuming a one-electron reduction. These reduction potentials for **5** and **7** are shifted anodically by 20−60 mV relative to nonsubstituted 5-coordinate $Cu^{II}-L_1$ complex, $[Cu^{II}(H_{-1}L_1)]^+$, **16** ($E_{pc} = -0.82$ V vs Ag/AgCl), indicating that the Cu^{I} complexes generated by electrochemical reduction are stabilized.

Conclusion

We have synthesized two synthetic bleomycin analogues, L_3 and L_4, to protect the oxidation of ligands from air. Their Cu^{II} complexes have been isolated and characterzed by X-ray crystallogphy. X-ray crystallography revealed that the successive replacement of hydrogen atoms by methyl groups on the carbon atoms changed the values of τ from 0.087 to 0.37, i.e. the coordination geometry around Cu^{II} changed from square-pyramidal toward the intermediate between trigaonal-bipyramidal and square-pyramidal. Moreover, the EPR and electronic data suggested that the geometry of Cu^{II} complexes were held in solution as well as in the solid state.

Finally, we demonstrated that the introduction of a methyl substituent into ethylene carbon atoms of L_1 could modulate the geometry, spectroscopic, and electronic properties of copper center, which are different from those of nonsubstituted $[Cu^{II}(H_{-1}L_1)]^+$, **16**.

Acknowledgment. This work supported by the Joint Studies Program (1997−1998) of the Institute for Moelcular Science.

Supporting Information Available: Listings of complete crystallographic data, positional and thermal parameters for hydrogen atoms, and bond distances and angles. This information is available free of charge via the Internet at http://pubs.acs.org.

IC980510I

(28) (a) Hathaway, B. J.; Dudley, R. J.; Nicholls, P. *J. Chem. Soc. A* **1969**, 1845. (b) Hathaway, B. J.; Procter, I. M.; Slade, R. C.; Tomlinson, A. A. *J. Chem. Soc. A* **1969**, 2219.
(29) Otsuka, M.; Yoshida, M.; Kobayashi, S.; Ohno, M.; Sugiura, Y.; Takita, T.; Umezawa, H. *J. Am. Chem. Soc.* **1981**, *103*, 6986.
(30) Miyoshi, K.; Tanaka, H.; Kimura, E.; Tsuboyama, S.; Murata, S.; Shimizu, H.; Ishizu, K. *Inorg. Chim. Acta* **1983**, *78*, 23.